RSC Advances

PAPER

View Article Online
View Journal | View Issue

Cite this: *RSC Adv.*, 2021, **11**, 35061

Effects of the Hubbard U correction on the electronic and magnetic properties of the tetragonal V_2P_2 sheet†

Yusuf Zuntu Abdullahi, *[a] Sohail Ahmad[b] and Abdullahi Abdu Ibrahim[c]

A recent theoretical work predicted the orthorhombic phase of the V_2P_2 sheet with the half-metallic electronic property using a linear combination of atomic orbitals (LCAO) basis set based on density functional theory (DFT). However, in the plane-wave DFT method, the tetragonal (t) V_2P_2 phase is the ground state structure. The total energy of the optimized tetragonal V_2P_2 is 0.91 eV per cell lower than that of the orthorhombic phase. Herein, we investigated the effects of Hubbard U correction onthe electronic, magnetic, and adsorption properties of the t-V_2P_2 sheet. The t-V_2P_2 sheet is found to be dynamically and mechanically stable. The t-V_2P_2 sheet prefers an antiferromagnetic ground state with an indirect narrowed bandgap of 0.23 eV. The estimated electron mobility in the t-V_2P_2 sheet at room temperature is approximately 24 times that of a hole. The t-V_2P_2 sheet exhibits a sizable magnetic anisotropy (MAE) of 69.63 μeV per V atom with in-plane magnetization. Mean-field approximation based on the 2D classical Heisenberg model predicts a high Néel temperature (T_N) of the t-V_2P_2 sheet up to 1263 K. The Li atom adsorption on the t-V_2P_2 sheet shows a transition from semiconductor to metal. Also the Li–V_2P_2 system has a residual integer magnetic moment of 1 μ_B. Due to strong steric coulomb repulsion, the minimum diffusion energy barrier (E_a) for the Li-ion on the t-V_2P_2 surface is high enough to make the Li atom immobile. Our findings demonstrate the potential of the t-V_2P_2 sheet for antiferromagnetic spintronics and sensing applications.

Received 12th October 2021
Accepted 21st October 2021

DOI: 10.1039/d1ra07558f

rsc.li/rsc-advances

1 Introduction

In recent years, basic and applied material investigations have been focused on the search for sustainable materials with revolutionary impacts on energy and related sectors. In this context, the target material should exhibit robust and controllable chemical and physical properties. Two-dimensional (2D) transition metal (TM) boride, popularly known as MBene[1] may be considered as one of the ideal classes of material to meet these requirements. Typical MBene examples are TM_2B_2 (TM = Mn, Mo, Fe, Cr) sheets.[2–5] Due to their appropriate electronic properties, they were found to be theoretically promising for spintronics, battery, and superconducting applications.[2,3,5] The Cr_2B_2 sheet was successfully synthesized[6,7] and first-principles calculations based on density functional theory (DFT) have confirmed the stability of the Cr_2B_2 sheet.[5]

Motivated by the potential of MBene,[2,8] it will be interesting to explore other new 2D materials with a similar MBene building block. As MBene has a dominant metal property, some questions arise: is it possible to create a new stable structure if the B atom of the MBene is replaced by another element? Would the metal property still be there? A recent report[9] showed that MnX (X = As, P) sheets with half-metallic properties can be used for high T_c ferromagnetic spintronics devices. Similar to MBene, the titanium boron nitride (Ti_2BN) sheet has been theoretically demonstrated for Li-ion battery (LIBs) with a capacity of about 889 mA h g^{-1}, 24, and 165 meV diffusion barrier of Li on the Ti_2BN surface and interlayer.[10] Moreover, a series of TM_2BC in bulk and monolayer forms have been shown to exhibit metallic properties with potential applications for superconducting, ceramic, and high T_c ferromagnetic spintronics.[11–14] It should be noted that these reported MnX (X = As, P), Ti_2BN and Ti_2BC materials have similar MBene building blocks in 2D and bulk forms. Therefore, it will be interesting to extend the search to other new 2D materials (similar to MBene). New 2D materials are expected to show new physical properties such as their MBene counterparts.

Herein, we are interested in studying the tetragonal (t) V_2P_2 sheet as a potential candidate for spintronic applications using first-principles calculations based on density functional theory (DFT)[15] plus Hubbard U[16] (DFT+U). Spin research on 2D

[a]Department of Physics, Faculty of Science, Kaduna State University, P.M.B. 2339, Kaduna State, Nigeria. E-mail: yusuf.zuntu@kasu.edu.ng
[b]Department of Physics, College of Science, King Khalid University, P O Box 9004, Abha, Saudi Arabia
[c]Computer Engineering Department, Altinbas University, Istanbul, Turkey

† Electronic supplementary information (ESI) available. See DOI: 10.1039/d1ra07558f

materials is currently one of the topics of high interest. The interest is the result of the recent experimental advancement in 2D magnetic nanostructures.[17,18] However, the low Curie (T_C) or Néel (T_N) temperature is a fundamental limit for their practical applications in spin-related devices. To deal with this problem, alternative 2D nanostructures with isotropic symmetry are theoretically examined for high T_C/T_N. Recent theoretical reports have shown that the tetragonal MnX (X = S, Sb) and hexagonal Mn_2C phases exhibit high Néel temperature with sizable magnetic anisotropy energy (MAE).[19,20] In a similar tetragonal phase, a T_C high above ambient temperature was observed with a considerable MAE for TM_2BC (TM = Cr, Mn) sheets.[14] These high T_N and T_C, potentials for 2D tetragonal structures mentioned above[14,19,20] prompted us to investigate the t-V_2P_2 sheet through a correct choice of computational method and symmetry.

So far, the previous work on V_2P_2 sheet has been limited only to the orthorhombic (o) phase.[21] In ref. 21 the o-V_2P_2 monolayer is ferromagnetic with semi-metallic electronic property using DFT[21] calculations. However, previous reports have shown that most MBene and related structures prefer the tetragonal phase as the ground state.[14,22] We are also aware that isotropic 2D materials which consist of TM atoms are among the most promising candidates for spintronics application.[22–24]

It is known that the spin-polarized DFT[15] within the framework of generalized-gradient approximations (GGA) for the exchange-correlation (xc) functional fail to provide reasonable results for the transition metal (TM) systems. To correct self-interaction errors that can be seen in this kind of TM-contained system, Coulomb interactions should be included by using Hubbard + U parameters in the calculations. This DFT+U[15,16] methods are commonly used to model this type of materials[22–24] as it produces greater accuracy of results compared to standard DFT at a moderate computational cost. In practice, there are different types of DFT+U approaches, but the most reliable one is to use the predictive method using the *ab initio* method based on the linear response approach (LRA).[16] The U parameter obtained using the LRA approach may not need to correspond to the experimental gap, but this approach improves the predictions of the band gap (beyond the standard DFT method) satisfactorily and is useful in cases where no previous data is available. The LRA approach has been used successfully for high-performance benchmarking of some well-known TM systems with greater accuracy that coincides with the available experimental data.[25]

In this study, we investigate the stability, electronic and magnetic properties of t-V_2P_2 sheet based on DFT+U calculations. The t-V_2P_2 sheet shows excellent vibrational and mechanical stabilities. We have also found that the AFM spin configuration corresponds to the ground state for the t-V_2P_2 sheet. The t-V_2P_2 exhibits a sizable magnetic anisotropy (MAE) of 69.63 μeV per V atom with an in-plane easy axis (EA). Mean-field approximation based on the 2D classical Heisenberg model predicts a high Néel temperature (T_N) of the t-V_2P_2 sheet up to 1263 K. The Li atom adsorption on the t-V_2P_2 sheet shows a transition from semiconductor to metal. Also the Li–V_2P_2 system leaves residual integer magnetic moment of 1 μ_B. Due to strong steric coulomb repulsion, minimum diffusion energy barriers (E_a) for Li-ion on the t-V_2P_2 surface is high enough to make the Li atom immobile.

2 Method

All calculations have been performed using DFT+U[15,16] as implemented in the plane-wave QUANTUM ESPRESSO (QE) package.[26] The generalized gradient approximation (GGA) of the Perdew–Burke–Enzerhof (PBE) functional has been used to account for the exchange-correlation potential.[27] The U value for t-V_2P_2 sheet has been evaluated using the LRA proposed by Cococcioni *et al.*[16] In the LRA estimations, the non-interacting (χ_0) and interacting (χ) density response functions of the system for localized perturbations were first obtained (see Fig. 1). The U_{eff} value is then estimated from the equation: $U_{eff} = (\chi_0^{-1} - \chi^{-1})$. Based on this expression, the estimated U_{eff} value for t-V_2P_2 is U_{eff} = 3.9 eV. Projected augmented-wave (PAW) pseudopotentials have been used to treat the electron-ion core interaction.[28] The van der Waals (vdW) correction has been included *via* the Grimme method of the DFT-D2 (ref. 29) using the PBE XC functional. The cut-off energies of 500 eV for the wave function and 5082 eV for the charge density have been used for all calculations. A 12 × 12 × 1 and 18 × 18 × 1 Mankhorst–Pack k-points have been used to sample the reciprocal space in the irreducible Brillouin zone (BZ) for self-consistency and total density of state computations respectively.[30] A vacuum space of 20 Å was imposed in the unit cell perpendicular direction to eliminate repeated image interaction of the t-V_2P_2 sheet. All atom's positions were fully relaxed until the remaining force on each atom was smaller than 0.002 eV $Å^{-1}$.

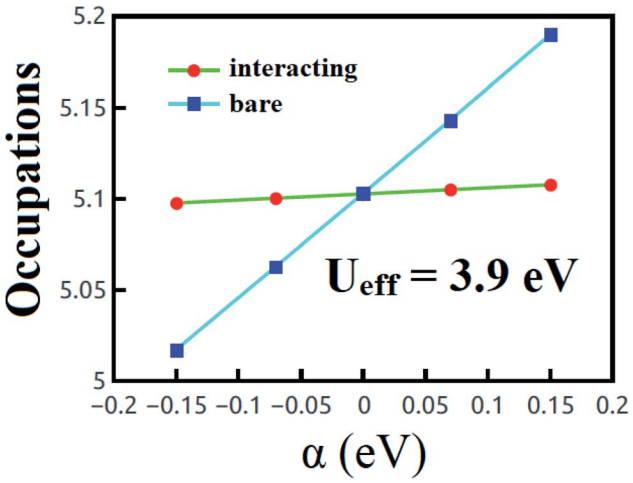

Fig. 1 The computed U_{eff} values for t-V_2P_2 sheet. The plot displays the dependence of the linear response of the d orbital occupation of V atom on potential shift α. The lines in the plots illustrate the non-interacting and the interacting inverse density response functions. The inverse response functions are obtained numerically by estimating the slope of the lines. χ_0 follows from the slope of the non-interacting line, whereas χ from the slope of the interacting line. The U_{eff} parameter is estimated from the equation presented in the Method section.

Table 1 Relative energies (E_R) for magnetic orientation of V_2P_2 sheet

	FM	AFM1	AFM2
E_R (eV)	1.31	1.98	0.00

3 Results and discussions

Firstly, we use PBE+D2+U to search for magnetically favorable configuration of the t-V_2P_2 sheet. An ferromagnetic (FM) and two antiferromagnetic states (AFM1 and AFM2) magnetic configurations in 2 × 2 supercell of t-V_2P_2 sheet has been considered (see Fig. 3). As listed in Table 1, the relative energy value illustrates AFM2 as the favorable magnetic ground state for t-V_2P_2 sheet. In AFM2, each V layer has parallel spins but opposite spins in the top and bottom V layers.

Therefore we use t-V_2P_2 unit cell with AFM2 configurations to compute the lattice parameters. An optimized t-V_2P_2 sheet is shown in Fig. 2(a). It can be viewed as a tetragonal structure with a space group of *P*4/*mmm* (no. 129). The black square line illustrates the top view of the t-V_2P_2 unit cell. The unit cell consists of two V and two P atoms. In the side view of Fig. 2(a), the P atom is located in the upper and lower regions of the sheet. Each atom in the sheet is chemically bonded by four neighboring atoms. The lattice constant ($a = b = 3.16$ Å, PBE) is found to be increased ($a = b = 3.36$ Å, PBE+U) when the Hubbard U correction was added. This indicates that the Hubbard U correction produces an expanded lattice constant which affects the ground state properties of t-V_2P_2 sheet. The optimized bond length in the *x*–*y* plane and the interlayer height (in the *z*-coordinate) is 2.48 Å and 2.68 Å respectively for the t-V_2P_2 sheet.

A recent theoretical study by Kadioglu[21] predicted the orthorhombic (o) phase of the t-V_2P_2 sheet with half-metallic electronic property. It was shown to hold promise for opto-electronic device applications. However, since the t-V_2P_2 sheet has not been realized experimentally, it is theoretically important to check other stable phases of the t-V_2P_2 sheet. This is necessary to avoid being trapped in the local minima. We clarify here the differences between the current study and the work reported in ref. 21 The ref. 21 used a linear combination of atomic orbitals (LCAO) in their calculations whereas we used the plane-wave basis set. As regards the Wyckoff's positions of atoms, the position of V atoms is different from that reported. These newly oriented V atoms tend to energetically favor tetragonal symmetry in the t-V_2P_2 sheet. The atomic Wyckoff positions for considered V_2P_2 structure in ref. 21 are similar to those reported in ref. 9 and 31, while in this study they can be found in ref. 14 and 19. The atomic positions and lattice constant for the tetragonal and orthorhombic V_2P_2 sheets are listed in Tables S1 and S2,† respectively. In addition, we use PBE plus Hubbard *U* corrections (PBE+U) in the current study, while in ref. 21 only PBE was used. We believe that precise estimates of ground-state properties in a material involving strongly correlated electrons can only be obtained if the Hubbard *U* correction is taken into account. We have also considered van der Waals (vdW) interactions *i.e.* PBE+U+D2, whereas ref. 21 does not include the vdW interactions for the V_2P_2 monolayer case. In ref. 21 it was reported that the o-V_2P_2 monolayer becomes unstable if vdW is included. However, most of the

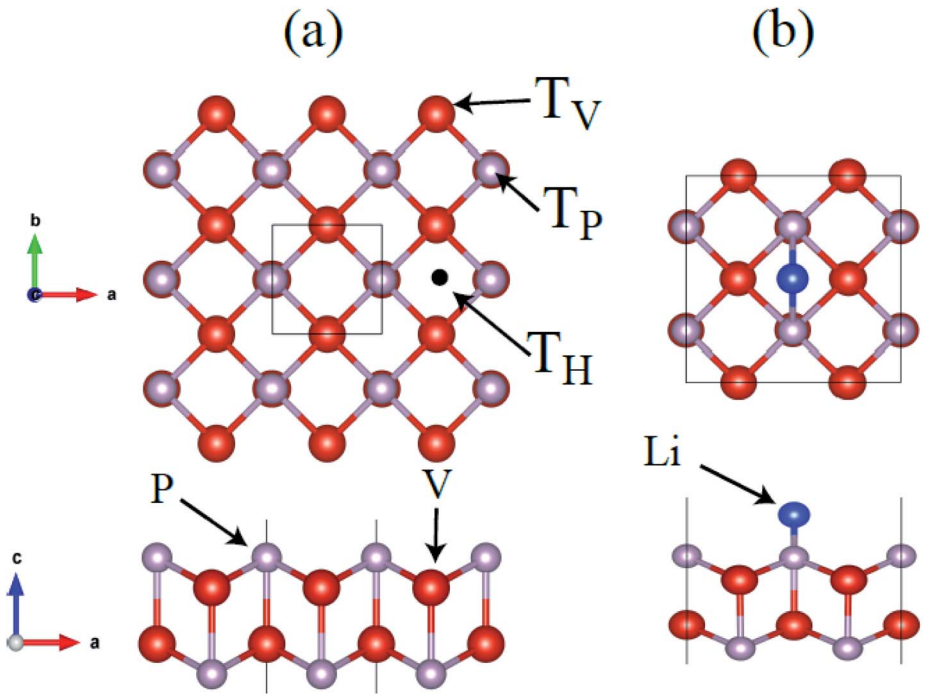

Fig. 2 (a) Top and side views for t-V_2P_2 sheet and stable adsorption sites are indicated on the surface of t-V_2P_2 sheet. (b) A typical example of top and side view for t-V_2P_2 sheet with adsorbed Li atom. Red, grey, purple balls represent the V, P, and Li atoms, respectively.

previous reports[22–24] of these kinds of 2D structures have considered vdW for the accurate estimates of ground-state properties.

To further substantiate our claims, the energy difference between orthorhombic and tetragonal V_2P_2 sheets have been evaluated and compared using the PBE method. We make sure that the same computational parameters are used to produce a negligible error in the results. The total energy of the optimized tetragonal V_2P_2 is 0.91 eV per cell more minimum than the orthorhombic phase (see Table S3†).

For comparison, the cohesive energy (E_{coh}) per atom of the t-V_2P_2 sheet is first evaluated using the PBE method. The E_{coh} is defined as follows;

$$E_{coh} = (nE_V + 2E_P - E_{t\text{-}V_2P_2})/4 \quad (1)$$

where $E_{t\text{-}V_2P_2}$ is the total energy of the t-V_2P_2 sheet, E_V, and E_P stand for the total energy of an isolated V and P atom in the unit cell respectively. The calculated E_{coh} is 6.42 eV for t-V_2P_2 sheet. This shows that the t-V_2P_2 sheet is the energetically more favorable phase than of reported orthorhombic V_2P_2 (5.22 eV) phase.[21] In addition, the E_{coh} of t-V_2P_2 sheet in this work is larger than that of the Cr_2B_2 (5.16 eV) and $CrRuB_2$ (6.06 eV) sheets[32] but comparable to tetr-Mo_2B_2 (6.49 eV) and tri-Mo_2B_2 (6.40 eV) sheets.[3]

To evaluate the possibility of experimental synthesis of the t-V_2P_2 sheet, we calculated the thermodynamic formation energy per atom which is expressed as

$$E_f = (E_{t\text{-}V_2P_2} - 2\mu_V - 2\mu_P)/4 \quad (2)$$

where μ_V, and μ_P denote the chemical potentials of V and P atoms, respectively. We estimate the chemical potentials of V and P atoms using $\mu_{V\text{ or }P} = E_{V\text{ or }P}/n$, where n is the number of V and P atoms in their bulk form with space group $m3m$ and $Imma$, respectively. The calculated E_f for t-V_2P_2 sheet is −0.55 eV per atom. The E_f is negative which indicates that the t-V_2P_2 sheet is thermodynamically stable and shows promise for experimental synthesis.

The strain-energy approach was used to estimate the in-plane stiffness (Y) and the Poisson's ratio (ν) of the t-V_2P_2 sheet. The strain-energy (E) as a function of strain (β) can be expressed as a quadratic polynomial that is defined as

$$E = \frac{1}{2}c_{11}\beta_{xx}^2 + \frac{1}{2}c_{22}\beta_{yy}^2 + c_{12}\beta_{xx}\beta_{yy}, \quad (3)$$

β_x, and β_y represent small strains along the a and b directions respectively. The linear elastic constants c_{11}, c_{22}, c_{12}, can be evaluated from eqn (4) and in eqn (5) equations. The second-order derivative is evaluated from fitted data points on E *vs.* β curves *via* an automatic interpolation scheme. The in-plane stiffness and Poisson's ratio are calculated using eqn (6) and (7), respectively.

Uni-axial

$$c_{11} = \frac{1}{A_0}\left(\frac{\partial^2 E_{11}}{\partial\beta^2}\right)\Big|_{s=0}, \quad (4)$$

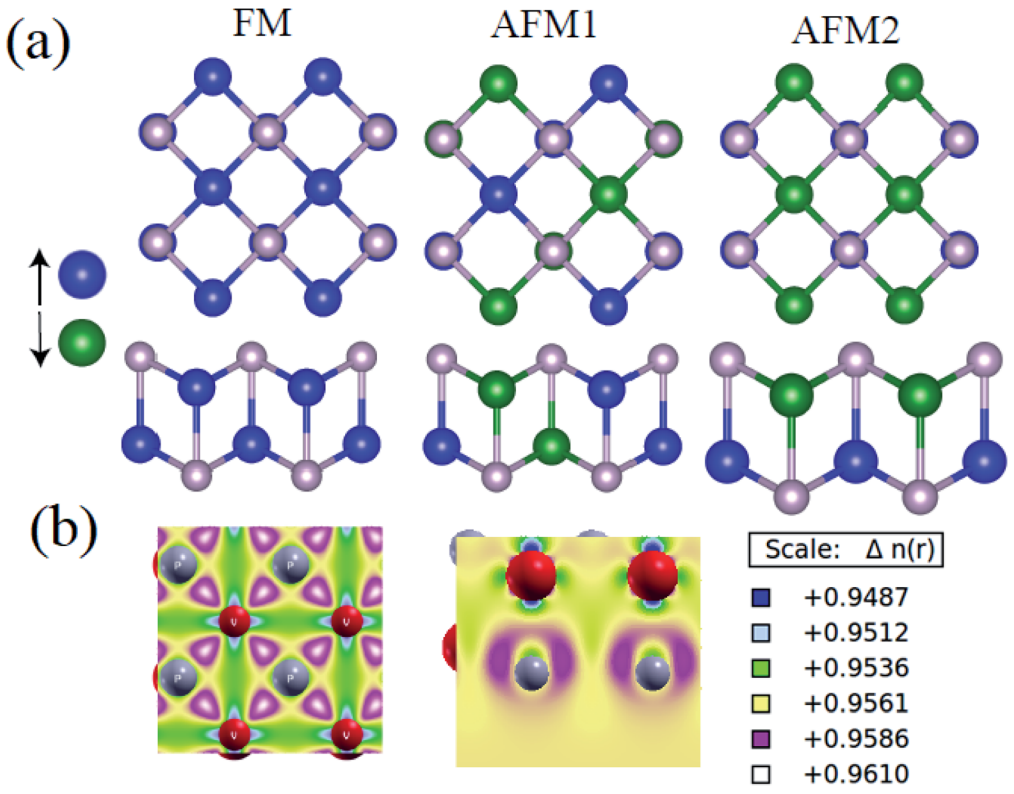

Fig. 3 (a) Typical example of magnetic structures of FM and two different AFM1, and AFM2 states for t-V_2P_2 sheet. Magnetic moments for each V atom in the FM, AFM1, and AFM2 states are approximately 2.27 μ_B 2.26 μ_B and 2.08 μ_B respectively. Blue and green colors stand for the spin up and spin down respectively. (b) The charge density difference in 2 × 2 supercell of t-V_2P_2 sheet.

Bi-axial

$$2(c_{11}+c_{12}) = \frac{1}{A_0}\left(\frac{\partial^2 E_{22}}{\partial \beta^2}\right)\Big|_{s=0}, \quad (5)$$

In-plane stiffness

$$Y = c_{11}(1-\nu^2), \quad (6)$$

Poisson's ratio

$$\nu = \frac{c_{12}}{c_{11}}, \quad (7)$$

A_0 is the equilibrium unit-cell area. The calculated Y and ν are 93.92 (93.92) N m^{-1} and 0.33 (0.33) along the a (b) directions, respectively. The values obtained show good isotropic tensile strength along the a and b direction. The estimated value for the Y is in accordance with B_2–C_6N_6 sheet (100.75 N m^{-1})[33] and T′-$ReTe_2$ sheet (94 N m^{-1})[34] along the perpendicular direction. In addition, the positive value of Y clearly illustrates the good mechanical stability of t-V_2P_2 sheet as defined for elastically stable materials.[35]

The phonon dispersion calculation has been carried out to ascertain the dynamic stability of t-V_2P_2 sheet. Fig. 4(a) displays the spectrum of phonons throughout the first Brillouin zone. The figure shows no imaginary frequencies for t-V_2P_2 sheet. The absence of imaginary frequencies confirms the dynamic stability of t-V_2P_2 sheet. On the right side of Fig. 4(a) is the atom projected phonon density of states (apPDOS). The apPDOS plot confirms that the lighter P atom vibrates with a frequency value greater than the heavier V atom. Overall, stability results demonstrate that the potential of the t-V_2P_2 sheet for real experimental synthesis.

The band structures and the corresponding atomic projected density of state (PDOS) of the t-V_2P_2 sheet is depicted in Fig. 3(b) and (c). The t-V_2P_2 sheet displays non-magnetic and metallic electronic properties using the PBE method (see Fig. 3(b)). An indirect bandgap of 0.233 eV with AFM as the preferred magnetic ground state (GS) is found when the Hubbard U (PBE+U method) correction is added. The Hubbard U correction produces a polarized spin in the 3d orbitals of the V atom after orbital reorientation. There is a magnetic moment of about 2.36 μ_B per V atom that is oriented in the antiparallel spins in the AFM GS. According to Hund's rules, an isolated V atom should have approximately 3 μ_B. However, due to bonding with neighboring P atoms in the t-V_2P_2 structure, the number of unpaired electrons of the 3d V orbit is reduced. This reduces the magnetic moment per V atom. Lowdin's charge analysis confirms that the magnetic moment of approximately 0.35 μ_B resides on each P atom in antiparallel spins. By plotting the charge density difference in Fig. 3(b), it is evident that the magnetic moment of t-V_2P_2 sheet is concentrated mainly in the V atoms. In AFM GS, the magnetic moment of V atoms couples in anti-parallel spins that have led to a zero magnetic moment. The metal to the semiconductor transition when U is added has been reported in a similar t-Mn_2S_2 structure.[19] Therefore, we hope the t-V_2P_2 sheet to exhibit semiconducting property when synthesized experimentally, as the PBE+U method is important in defining the actual electronic property of a system involving strongly correlated electrons. From the PDOS plot of t-V_2P_2 sheet, the contributions of the p, and d-orbitals of the P and V atoms respectively dominate both the valence band maximum (VBM) and conduction band minimum (CBM). We further performed the HSE06 hybrid functional calculations and found not much difference with the results obtained from PBE+D2+U. The HSE06 band structure has been included in the ESI (Fig. S2†) showing a narrow band of about 0.20 eV which is comparable to PBE+D2+U. In addition, the magnetic moment of about 0.02 μ_B obtained from the HSE06 calculation further confirms the AFM ground state.

Based on the deformation potential (E_d) model,[36] the carrier mobility of t-V_2P_2 sheet can be estimated using the expression defined as;

$$\mu = \frac{2eh^3C}{3k_BT|m^*|^2E_d^2} \quad (8)$$

Here, k_B, T (300 K) and h are the Boltzmann constant, room temperature and reduced plank constant. C is the in-plane

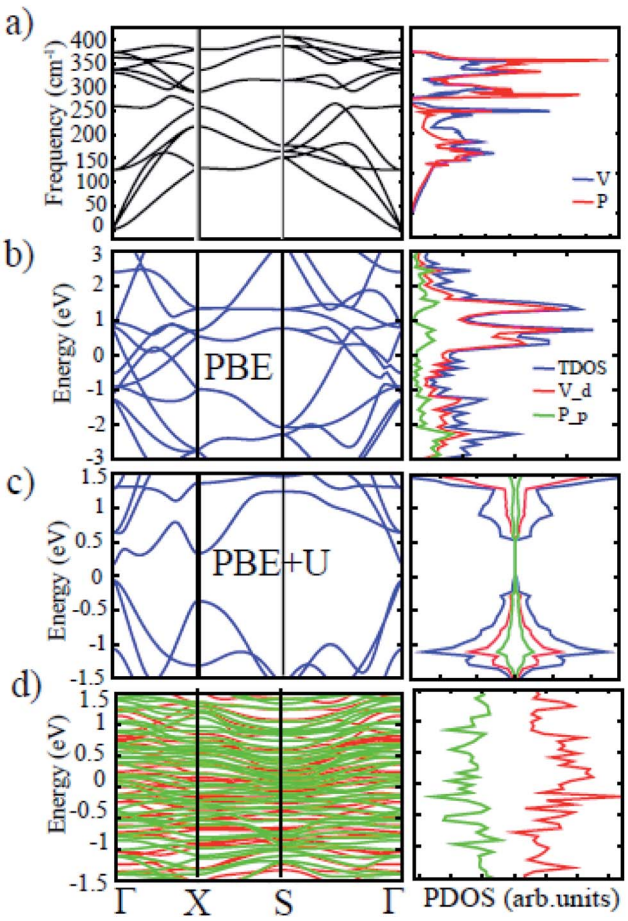

Fig. 4 (a) The phonon dispersions curves and the corresponding aPDOS. The electronic band structure and PDOS obtained using the (b) PBE and (c) PBE+U for t-V_2P_2 sheet. (d) The electronic band structure and TDOS were obtained using the PBE+U for t-V_2P_2 with adsorbed Li atom. The red and green colors represent spin-up and spin-down.

stiffness that has been estimated in the previous paragraph. E_d is the linear slope fitted to the CBM and VBM energies as a function of uniaxial tensile strain. The effective mass $m^* = \pm\hbar^2\left(\frac{d^2E_k}{dk^2}\right)^{-1}$ is evaluated from fitted data points on E–k curves *via* an automatic interpolation scheme. The data points were selected from the band portion closed to the CBM or VBM (see Fig. S2†). The slopes of each E–k curves give the coefficient for the parabolic terms which is then used to estimate the m^* for holes and electrons at the VBM and CBM respectively. Our estimated results show that the holes are heavier than electrons for t-V_2P_2 sheet (see Table S4†). Consequently, the electron mobility in this t-V_2P_2 sheet at room temperature is approximately 24 times that of the hole.

Magnetic anisotropy energy (MAE) calculations have been carried to determine the favorable magnetization directions on t-V_2P_2 sheet. It should be noted that the non-collinear spin-polarized with spin–orbit coupling (SOC) has been included in the MAE calculations. The relative energy values for the magnetization directions are summarized in Table 2, namely four in-plane ([100], [010], [110], [111]) and an out-of-plane [001] magnetization direction have been considered. A positive relative energy value shows a favorable magnetization easy axis of the system. As listed in Table 2, the t-V_2P_2 sheet favors in-plane [100]/[010] magnetization direction. The estimated in-plane MAE of t-V_2P_2 sheet is $E([001]) - E[100] = 69.63$ μeV per V atom. The value is almost the same as the reported Mn_2C sheet[20] (69 μeV per V atom) and the easy axis of the Mn_2C sheets is equally in the in-plane [100] direction.

Next, we investigate the magnetic properties of the t-V_2P_2 sheet. Looking at the obtained results, the t-V_2P_2 sheet can be modeled by $J_1 - J_2$ Heisenberg Hamiltonian expressed as:

$$\mathcal{H} = -J_1\sum_{ij_1}\alpha_i\alpha_j - J_2\sum_{ik_1}\alpha_i\alpha_k - K_x\sum_i(\alpha_i^x)^2 - K_y\sum_i(\alpha_i^y)^2 - K_z\sum_i(\alpha_i^z)^2 \quad (9)$$

The first and second terms are summations over the nearest and next-nearest neighbor spin pairs, respectively. J_1 and J_2 denote the antiferromagnetic exchange interaction between nearest neighbors and next-nearest neighbors, respectively. Here, the exchange interaction terms of the V_2P_2 sheet depends on the number of J_1 and J_2 bond distances. α_i is the magnetic moment of V atom taken from the favorable magnetic configuration (AFM2 in this case) of the V_2P_2 sheet. K_x, K_y and K_z represent the uniaxial magnetic anisotropy constants in x, y and z directions, respectively. The K_z factor is neglected since the preferred magnetization direction is along [100]/[010] for the V_2P_2 sheet.

Table 2 Magnetic anisotropy energy (MAE) in μeV (per unit cell) for V_2P_2 sheet. The easy axis (EA) is within the basal plane [100]. V_2P_2 sheet has AFM as the ground state

MAE	EA
$E(010) - E(100)$	0.00
$E(001) - E(100)$	557.00
$E(110) - E(100)$	1.00
$E(111) - E(100)$	187.50

Based on the (2 × 2) V_2P_2 unit cell, the analysis of the three magnetic states, FM, AFM1 and AFM2 in terms of their energies E(FM), E(AFM1) and E(AFM2), respectively can be derived as follows:

$$E(\mathrm{FM}) = E_0 - 9J_1\alpha^2 - 8J_2\alpha^2 \quad (10)$$

$$E(\mathrm{AFM1}) = E_0 + J_1\alpha^2 + 8J_2\alpha^2 \quad (11)$$

$$E(\mathrm{AFM2}) = E_0 + 9J_1\alpha^2 - 8J_2\alpha^2. \quad (12)$$

E_0 denotes the free magnetic coupling energy and α is the magnetic dipole moment of the V atom. By benefiting from eqn (10)–(12), exchange interaction parameters, J_1 and J_2 can be written as:

$$J_1 = -\frac{E(\mathrm{FM}) - E(\mathrm{AFM2})}{18\alpha^2} \quad (13)$$

$$J_2 = -\frac{4E(\mathrm{FM}) - 9E(\mathrm{AFM1}) + 5E(\mathrm{AFM2})}{144\alpha^2} \quad (14)$$

Using eqn (11) and (12) given above, the exchange parameters J_1 and J_2 were estimated to be −16.86 meV/$\alpha_B{}^2$ and −20.37 meV/$\alpha_B{}^2$ respectively. These J_1 and J_2 values can be used to estimate the T_N of t-V_2P_2 sheet using Monte Carlo simulations based on the Heisenberg model.

However, within the mean-filed approximation, the Néel temperature for an AFM state can be estimated as

$$T_N = 2E_R/3k_BN \quad (15)$$

where E_R and N denote the relative between AFM and FM states and the number of magnetic atoms in the unit cell. The Boltzmann constant k_B is taken as $1.38064852 \times 10^{-23}$ J K^{-1}. The obtained T_N of t-V_2P_2 sheet is 1263 K, which is overestimated. It should be noted that the t-V_2P_2 sheet has an in-plane magnetic anisotropy. Such an in-plane anisotropy shows that the magnetic state of the t-V_2P_2 sheet is a limiting case of the Heisenberg model: XY-model. According to the Mermin Wagner theorem, the 2D systems with continuous symmetry cannot have a long-range order at a finite temperature.[37] In 2D, the XY model shows the very unique Kosterlitz–Thouless (KT) transition for which conventional methods of critical phenomena are not very useful.[38] Therefore, the determination of the KT phase transition for the t-V_2P_2 sheet can be the subject of a detailed investigation in future work.[39–41]

We further explore the Li atom adsorption and diffusion properties on t-V_2P_2 sheet. We begin with the search for the single Li atom favorable high-symmetric adsorption site (Ads. site) on the V_2P_2 sheet. Based on the tetragonal symmetry of t-V_2P_2 sheet, three Ads. site has been considered on (2 × 2) supercell of t-V_2P_2 sheet, *i.e.* for the Li atom at the top of the V (T_V), P (T_H), atoms and hollow (T_H) sites (see Fig. 4). All atoms in

the t-V_2P_2 with adsorbed Li (Li–V_2P_2) are fully relaxed without any geometry constraint. There is no sign of reconstruction (see Fig. 2) after full structural optimization and top of the V (T_V) is energetically favorable Ads. site for Li atom on t-V_2P_2. To estimate the favorable magnetic ground state, ferromagnetic (FM) and antiferromagnetic (AFM) calculations have been performed for Li–V_2P_2 system. The AFM configuration has parallel spins within each layer of V, but opposite spins in the upper and lower layer of V. Our PBE+D2+U calculation favors antiferromagnetic configuration with an energy difference of about 1.14 eV as compared with ferromagnetic calculation. Moreover, both PBE+D2 and PBE+D2+U have been considered for the Li–V_2P_2 with adsorbed Li system phonon calculations. The plot shows no imaginary modes for PBE+D2 and a negligible numerical noise for the PBE+D2+U case. The results confirm the dynamic stability of Li–V_2P_2 system (see Fig. S4†).

The adsorption energy (E_{ads}) of Li–V_2P_2 system can be calculated as,

$$E_{ads} = (E_{V_2P_2} + E_{Li}) - E_{Li-V_2P_2}, \quad (16)$$

Here, $E_{Li-V_2P_2}$, $E_{V_2P_2}$ and E_{Li} represent the total energy of $E_{Li-V_2P_2}$, the energy of the $E_{V_2P_2}$, and that of an isolated Li atom, respectively. Based on the estimated positive E_{ads} (2.38 eV) value, Li atom strongly chemisorbed on the t-V_2P_2 surfaces. Correspondingly, the bond length (d) between t-V_2P_2 surface and the Li adatom is 2.46 Å. As displayed in Fig. 4(d), the spin-polarized band structure and the corresponding TDOS of Li–V_2P_2 system shows the populated bands across the Fermi level. This means Li atom adsorption on t-V_2P_2 sheet exhibit a semiconductor to metal transition. Also the Li–V_2P_2 system leaves residual integer magnetic moment of 1 μ_B. This indicates that the valence electrons of the adsorbed Li atom remain localized and couple in the parallel spin state, thus inducing a magnetic moment. We also calculated the geometric, electronic, magnetic, and adsorption energies of energetically stable structures of t-V_2P_2 with adsorbed Li, Na, K, Si, and Ge atoms using the PBE+D2 method. Their results are provided in Table S5 in the ESI† part. As summarized in Table S5,† the calculated positive E_{ads} values show that all Li, Na, K, Si, and Ge atoms chemisorbed on the t-V_2P_2 surfaces. Interestingly, the Li–V_2P_2, Na–V_2P_2 and K–V_2P_2 structures display metallic electronic properties with the residual magnetic moment, whereas the remaining Si–V_2P_2 and Ge–V_2P_2 are non-magnetic metals.

We further investigate the diffusion pathway and energy barrier of Li-ion on the t-V_2P_2 surface. The calculation in this section has been performed using the CI-NEB approach. Only one minimum pathway has been considered for Li-ion diffusion on the t-V_2P_2 surface. The pathway is chosen according to the preferred above-mentioned high-symmetric adsorption site for Li. As illustrated in Fig. 5, the deduced minimum diffusion energy barriers (E_a) for Li-ion on t-V_2P_2 the sheet is approximately 8 eV. The estimated E_a for Li on t-V_2P_2 surface indicate a strong interaction between Li and the surrounding atoms in the t-V_2P_2 sheet. This steric coulomb effect provided by the t-V_2P_2 surface atoms impact the Li diffusion on the t-V_2P_2 surface and hence the higher E_a is needed for the Li diffusion. The high value of E_a for Li on t-V_2P_2 indicates that Li–V_2P_2 may not be a suitable candidate for Li-ion battery (LIBs) anode electrode. However, t-V_2P_2 can be proposed as a good candidate for sensing application.

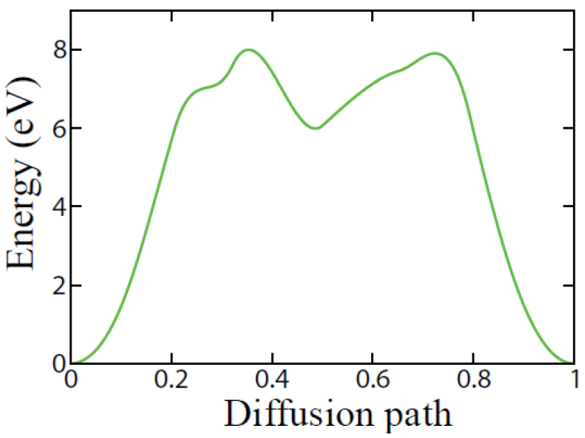

Fig. 5 Diffusion energy barriers of Li on the t-V_2P_2 sheet.

4 Conclusions

In conclusion, we presented theoretical results on the electronic, magnetic, and adsorption properties of new t-V_2P_2 sheet using a DFT+U. The t-V_2P_2 sheet is found to be dynamically and mechanically stable. The t-V_2P_2 sheet prefers an antiferromagnetic ground state with an indirect narrowed bandgap of 0.23 eV. The estimated electron mobility in the t-V_2P_2 sheet at room temperature is approximately 24 times that of a hole. The t-V_2P_2 sheet exhibits a sizable magnetic anisotropy (MAE) of 69 μeV per V atom with in-plane magnetization. Mean-field approximation based on the 2D classical Heisenberg model predicts a high Néel temperature (T_N) of the t-V_2P_2 sheet up to 1263 K. The Li atom adsorption on the t-V_2P_2 sheet shows a transition from semiconductor to metal. Also the Li–V_2P_2 system leaves residual integer magnetic moment of 1 μ_B. Due to strong steric coulomb repulsion, minimum diffusion energy barriers (E_a) for Li-ion on the t-V_2P_2 surface is high enough to make the Li atom immobile. Finally, our theoretical results indicate the potential of the t-V_2P_2 sheet for antiferromagnetic spintronics and sensing applications.

Conflicts of interest

There are no conflicts to declare.

Acknowledgements

Sohail Ahmad extends his appreciation to the Deanship of Scientific Research at King Khalid University for financial support through the research groups program under grant number (R. G. P. 2/188/42). We would like to acknowledge Prof. Dr Ethem Akturk and Prof. Dr Olcay Üzengi Aktürka from the Department of Physics and Department of Electrical and Electronic Engineering, Adnan Menderes University, Aydın, Turkey

for providing the computing resources to carry out part of the calculations done in this paper.

References

1 M. Khazaei, J. Wang, M. Estili, A. Ranjbar, S. Suehara, M. Arai, K. Esfarjani and S. Yunoki, *Nanoscale*, 2019, **11**, 11305–11314.
2 Y. Zuntu Abdullahi, Z. Demir Vatansever, E. Aktürk, Ü. Akıncı and O. Üzengi Aktürk, *Phys. Chem. Chem. Phys.*, 2020, **22**, 10893–10899.
3 T. Bo, P.-F. Liu, J. Zhang, F. Wang and B.-T. Wang, *Phys. Chem. Chem. Phys.*, 2019, **21**, 5178–5188.
4 Z. Guo, J. Zhou and Z. Sun, *J. Mater. Chem. A*, 2017, **5**, 23530–23535.
5 T. Bo, P.-F. Liu, J. Xu, J. Zhang, Y. Chen, O. Eriksson, F. Wang and B.-T. Wang, *Phys. Chem. Chem. Phys.*, 2018, **20**, 22168–22178.
6 H. Zhang, H. Xiang, F.-z. Dai, Z. Zhang and Y. Zhou, *J. Mater. Sci. Technol.*, 2018, **34**, 2022–2026.
7 H. Zhang, F.-Z. Dai, H. Xiang, X. Wang, Z. Zhang and Y. Zhou, *J. Mater. Sci. Technol.*, 2019, **35**, 1593–1600.
8 G. Yuan, T. Bo, X. Qi, P.-F. Liu, Z. Huang and B.-T. Wang, *Appl. Surf. Sci.*, 2019, **480**, 448–453.
9 B. Wang, Y. Zhang, L. Ma, Q. Wu, Y. Guo, X. Zhang and J. Wang, *Nanoscale*, 2019, **11**, 4204–4209.
10 Y.-Y. Wu, T. Bo, X. Zhu, Z. Wang, J. Wu, Y. Li and B.-T. Wang, *Appl. Surf. Sci.*, 2020, **513**, 145821.
11 R. Escamilla, E. Carvajal, M. Cruz-Irisson, F. Morales, L. Huerta and E. Verdin, *J. Mater. Sci.*, 2016, **51**, 6411–6418.
12 H. Bolvardi, J. Emmerlich, D. Music, J. von Appen, R. Dronskowski and J. Schneider, *J. Phys.: Condens. Matter*, 2012, **25**, 045501.
13 P. Barua, M. Hossain, M. Ali, M. Uddin, S. Naqib and A. Islam, *J. Alloys Compd.*, 2019, **770**, 523–534.
14 Y. Z. Abdullahi, Z. D. Vatansever, F. Ersan, U. Akinci, O. U. Akturk and E. Akturk, *Phys. Chem. Chem. Phys.*, 2021, **23**, 6107–6115.
15 P. Hohenberg and W. Kohn, Inhomogeneous electron gas, *Phys. Rev.*, 1964, **136**, B864.
16 M. Cococcioni and S. De Gironcoli, *Phys. Rev. B: Condens. Matter Mater. Phys.*, 2005, **71**, 035105.
17 B. Huang, G. Clark, E. Navarro-Moratalla, D. R. Klein, R. Cheng, K. L. Seyler, D. Zhong, E. Schmidgall, M. A. McGuire and D. H. Cobden, *Nature*, 2017, **546**, 270.
18 Z. Fei, B. Huang, P. Malinowski, W. Wang, T. Song, J. Sanchez, W. Yao, D. Xiao, X. Zhu and A. F. May, *Nat. Mater.*, 2018, **17**, 778.
19 Y. Z. Abdullahi, F. Ersan, Z. D. Vatansever, E. Aktürk and O. Ü. Aktürk, *J. Appl. Phys.*, 2020, **128**, 113903.
20 L. Hu, X. Wu and J. Yang, *Nanoscale*, 2016, **8**, 12939–12945.
21 Y. Kadioglu, *Mater. Sci. Eng., B*, 2021, **268**, 115111.
22 T. Bo, P. F. Liu, J. Zhang, F. Wang and B. T. Wang, *Phys. Chem. Chem. Phys.*, 2019, **21**, 5178–5188.
23 Y. Z. Abdullahi and S. Ahmad, *Phys. Chem. Chem. Phys.*, 2021, **23**, 16316–16323.
24 T. Gorkan, E. Vatansever, Ü. Akıncı, G. Gökoğlu, E. Aktürk and S. Ciraci, *J. Phys. Chem. C*, 2020, **124**, 12816–12823.
25 N. E. Kirchner-Hall, W. Zhao, Y. Xiong, L. Timrov and I. Dabo, *Appl. Sci.*, 2021, **11**, 2395.
26 P. Giannozzi, S. Baroni, N. Bonini, M. Calandra, R. Car, C. Cavazzoni, D. Ceresoli, G. L. Chiarotti, M. Cococcioni and I. Dabo, *J. Phys.: Condens. Matter*, 2009, **21**, 395502.
27 J. P. Perdew, K. Burke and M. Ernzerhof, *Phys. Rev. Lett.*, 1996, **77**, 3865.
28 G. Kresse and D. Joubert, *Phys. Rev. B: Condens. Matter Mater. Phys.*, 1999, **59**, 1758.
29 S. Grimme, J. Antony, S. Ehrlich and H. Krieg, *J. Chem. Phys.*, 2010, **132**, 154104.
30 H. J. Monkhorst and J. D. Pack, *Phys. Rev. B: Solid State*, 1976, **13**, 5188.
31 A. V. Kuklin, S. A. Shostak and A. A. Kuzubov, *J. Phys. Chem. Lett.*, 2018, **9**, 1422–1428.
32 Y. Z. Abdullahi, Z. D. Vatansever, E. Aktürk, Ü. Akıncı and O. Ü. Aktürk, *Phys. Status Solidi B*, 2020, 2000396.
33 Y. Z. Abdullahi, T. L. Yoon and A. A. Kassimu, *Mater. Chem. Phys.*, 2020, **254**, 123470.
34 M. Yagmurcukardes, *Turk. J. Phys.*, 2020, **44**, 450–457, DOI: 10.3906/fiz-2004-17.
35 F. Mouhat and F.-X. Coudert, *Phys. Rev. B: Condens. Matter Mater. Phys.*, 2014, **90**, 224104.
36 J. Bardeen and W. Shockley, *Phys. Rev.*, 1950, **80**, 72.
37 N. D. Mermin and H. Wagner, *Phys. Rev. Lett.*, 1966, **17**, 1133–1136.
38 J. M. Kosterlit and D. J. Thouless, *J. Phys. C: Solid State Phys.*, 1973, **6**, 1181–1203.
39 S. Tiwari, M. L. Van de Put, B. Sorée and W. G. Vandenberghe, *npj 2D Mater. Appl.*, 2021, **5**, 1–7.
40 Y.-D. Hsieh, Y.-J. Kao and A. W. Sandvik, *J. Stat. Mech.: Theory Exp.*, 2013, P09001.
41 J. M. Kosterlitz, *Rep. Prog. Phys.*, 2016, **79**, 026001.